Synthesis, crystal structure and optical investigation of the new phosphates: $Na_7Mg_{13}Ln(PO_4)_{12}$ (Ln=La, Eu)

Hasna Jerbi [a], Mourad Hidouri [a], Benoit Glorieux [b], Jacques Darriet [b], Alain Garcia [b], Véronique Jubera [b], Mongi Ben Amara [a,*]

[a] UR: Matériaux Inorganiques, Département de Chimie, Faculté des Sciences, 5019 Monastir, Tunisie
[b] CNRS, Université de Bordeaux, ICMCB, 87 avenue du Dr. A. Schweitzer, Pessac, F-33608, France

ARTICLE INFO

ABSTRACT

Two new isostructural rare earth phosphates $Na_7Mg_{13}Ln(PO_4)_{12}$ (Ln=La, Eu) have been synthesized and investigated by X-ray diffraction and optical measurements. They crystallize in the orthorhombic system with the $Cmc2_1$ space group (Z=4). The crystal structure exhibits a new type of framework built up from LnO_8 (Ln=La, Eu), MO_6 (M=0.5Mg+0.5Na) and MgO_x (x=5, 6) polyhedra and PO_4 tetrahedra linked by common corner, edge or face. It can be described in terms of $[Mg_4MP_4O_{22}]_\infty$ layers stacked along the a direction. These layers are interconnected by $[Mg_4LnP_4O_{36}]_\infty$ undulating chains spreading along the b direction. This framework delimits 6 distinct cavities occupied by Na^+ cations. The results of the optical study of $Na_7Mg_{13}La_{1-x}Eu_x(PO_4)_{12}$ (x=0, 0.02, 0.1, 1) reveal the presence of two different Eu^{3+} ion environments whereas the X-ray study predicts the existence of only one Eu site. This difference can be explained by the possible presence of the europium element in the sodium sites with small occupancies which cannot be detected by the X-ray structural determination.

1. Introduction

For a long time, inorganic phosphate materials have been the focus of intensive research for their attractive crystal chemistry and striking properties [1]. Those containing rare earth elements are of special interest as prospective candidates for optical applications [2]. Recently, some of them were deeply investigated for white light-emitting diode (LEDs), in a context of energy saving, for use in next generation solid-state illumination devices, backlighting, screening, etc. [3]. The current performances of white LEDs are due to the combination of a blue chip $Ga_{1-x}In_xN$ with yellow phosphor $Y_3Al_5O_{12}$:Ce^{3+} [4]. Even if the efficiency is acceptable, the color rendering index (the color rendering index CRI is characterized by comparing the color points of a set of test colors under illumination with the lamp to be tested and a black body radiator). The color rendering index (CRI) equals 100 if the color points are the same under illumination with both sources is the failure point of the commercial use of daily lighting [5].

In order to obtain a warm white light, the new technologies are based on the combination of a blue diode with two red and green phosphors (R, G) [6] or the combination of a U.V. diode with three phosphors emitting at the primary colors (RGB) [7]. If the blue and the green luminescence start to be well established [8], the red

emission is still not fully optimized, because of the low quantum yield of the actual red phosphors [9]. In this context, phosphates are investigated because of their low cost, their high stability for use in lamp applications and their important crystallographic possibilities to accommodate luminescent ions [10]. More precisely, trivalent europium can be easily introduced in those matrices by substitution of alkaline, alkaline earth or rare earth elements giving rise to suitable red emission [11].

As a part of our research activity devoted to the synthesis and characterization of new optically interesting rare earth phosphates in the quest of new phosphorus materials used in lighting devices [12], we recently started a systematic exploratory study of the Na_3PO_4–$M_3(PO_4)_2$–$LnPO_4$ (M=Mg, Ca, Sr) pseudo-systems. We describe here the synthesis and the original structure of the $Na_7Mg_{13}Ln(PO_4)_{12}$ (Ln=La, Eu) phosphates and we also investigate the optical properties of $Na_7Mg_{13}La_{1-x}Eu_x(PO_4)_{12}$ (x=0, 0.02, 0.1, 1) in order to determine its spectral distribution. A study on the real location of the rare earth element is also reported.

2. Experimental section

2.1. Synthesis

Single crystals of the $Na_7Mg_{13}La(PO_4)_{12}$ and $Na_7Mg_{13}Eu(PO_4)_{12}$ compounds were grown in a flux of sodium molybdate Na_2MoO_4 starting from mixtures of Na_2CO_3, $MgCO_3$, Ln_2O_3 (Ln=La, Eu),

$NH_4H_2PO_4$ and $Na_2MoO_4 \cdot 2H_2O$ in a molar ratio of 2.5:14:0.5:12:6. All the reactants were of analytical grade and were used without further purification. Each mixture was ground in an agate mortar to ensure its best homogeneity and reactivity. Then, it was heated in a platinum crucible for 24 h at 673 K to expel H_2O, CO_2 and NH_3. After intermediate grinding, the uniform product was melted for 2 h at 1273 K and subsequently cooled down to 773 K with a $10° h^{-1}$ rate, after which the furnace was turned off. Hexagonally shaped crystals were obtained by washing the whole product with warm water. Their elemental analysis by ICP indicated the exclusive presence of Na, Ln, Mg and P in atomic ratios of $Na:Mg:La:P \approx 7.4(2):13.2(2):0.95(5):12(2)$ for $Na_7Mg_{13}La(PO_4)_{12}$ and $Na:Mg:Eu:P \approx 7.1(2):13.6(2):0.97(5):12(2)$ for $Na_7Mg_{13}Eu(PO_4)_{12}$, in accordance with the $Na_7Mg_{13}Ln(PO_4)_{12}$ composition.

After the structural determination, four pure powder samples of $Na_7Mg_{13}La_{1-x}Eu_x(PO_4)_{12}$, namely $Na_7Mg_{13}La(PO_4)_{12}$ (NML), $Na_7Mg_{13}La_{0.98}Eu_{0.02}(PO_4)_{12}$ (NMLEu2), $Na_7Mg_{13}La_{0.9}Eu_{0.1}(PO_4)_{12}$ (NMLEu10) and $Na_7Mg_{13}Eu(PO_4)_{12}$ (NMEu) were synthesized by the Pechini method [13] according to the following procedure. First, appropriate amounts of La_2O_3 (Eu_2O_3) and $MgCO_3$ (molar ratio 0.5:13) are dissolved in nitric acid. Once the dissolution is achieved, Na_2CO_3 and $NH_4H_2PO_4$ (molar ratio 3.5:12) are added. Later, 0.22 g of citric acid and 0.1 g of ethylene glycol are added. The obtained limpid solution is kept at 333 K for 8 h under continuous stirring leading to the formation of a randomly polymeric resin in which cations are uniformly distributed. Subsequently, this resin is heated at 423 K to breakdown the formed polymer. The final step in this procedure is calcinations for 12 h at 673 K, for 12 h at 873 K, then for 24 h at 1073 K.

2.2. X-ray study

The purity of the synthesized powders was checked by the examination of their X-ray powder diagrams collected in the range $5° \leq 2\theta \leq 80°$ on a PANalytical diffractometer using CuK_α radiation ($\lambda = 1.5406$ Å).

The structure was determined using a crystal of dimensions $0.32 \times 0.18 \times 0.16$ mm^3, selected from the $Na_7Mg_{13}Eu(PO_4)_{12}$ preparation. Data collection was performed by a CAD4 Enraf Nonius diffractometer using the MoK_α radiation ($\lambda = 0.71073$ Å), according to the conditions summarized in Table 1.

2.3. Optical measurements

Photoluminescent properties were analyzed using a spectro-fluorimeter SPEX FL212. Excitation spectra were corrected for the variation of the incident flux as well as emission spectra for the transmission of the monochromator and the response of the photomultiplier. This equipment is composed of a 450 W xenon lamp, an excitation double monochromator, a sample holder, an emission double monochromator and a thermoelectricity cooled photomultiplier tube.

This equipment was used to record diffuse reflectance spectra. In this case, the emission and the excitation monochromator are set in a synchronous mode, in order to collect all the diffuse reflection of the xenon lamp without catching any fluorescence photon. A black reference (B: black toner) and a white reference (W: Magnesia MgO) were scanned in the same condition and the measurement from the sample (S) was corrected following this relation, in order to obtain the desired data (D): $D = (S-B)/(W-B)$.

This equipment was also used to perform low temperature measurements, using a specific sample holder surrounded by a liquid nitrogen device, in order to maintain the sample at 80 K.

Table 1

Crystal data and experimental conditions for the structural determination of $Na_7Mg_{13}Eu(PO_4)_{12}$.

Crystal Data	
Chemical formula	$Na_7Mg_{13}Eu(PO_4)_{12}$
Space group	$Cmc2_1$
a(Å)	10.275(9)
b(Å)	15.446(2)
c(Å)	23.386(2)
Z	4
ρ_{cal} (g cm^{-3})	3.16
Intensity measurements	
Crystal dimensions (mm)	$0.32 \times 0.18 \times 0.16$
Apparatus	CAD4 Enraf Nonius
λ MoKα (Å)	0.71073
Monochromator	Graphite
μ (mm^{-1})	2.67
Scan mode	$\omega/2\theta$
$2\theta_{max}$	60°
Unique reflections; R_{int}	3002; 0.046
Observed reflections ($F_0 > 4\sigma(F_0)$)	2856
Indices	$-1 \leq h \leq 14, \ -1 \leq k \leq 21, \ -1 \leq l \leq 32$
$F(000)$	3440
Structure solution and refinement	
Intensity correction	Lorentz and polarization
Absorption correction	Ψ-scan
T_{min}, T_{max}	0.586; 0.651
Resolution method	Direct method
Agreement factors $[F_0 > 4\sigma(F_0)]$	$R_1 = 0.025$; w$R_2 = 0.059$; $S = 1.12$
Number of refined parameters	434
Weighting scheme	$w = 1/[\sigma^2(F_0^2) + 0.0283P)^2 + 19.2374P]$ where $P = (F_0^2 + 2F_c^2)/3$
$(\Delta\rho)_{max,min}$(e Å^{-3})	1.107; -1.176

3. Results and discussion

3.1. Determination and description of the structure

The powder X-ray patterns reported in Fig. 1 indicate the formation of a continuous solid solution between lanthanum and europium in the composition range $0 \leq x \leq 1$. The refined cell parameters are indicated in Table 2.

The structure was solved in the $Cmc2_1$ space group by application of direct methods [14] which established one symmetry distinct position for the Eu atoms. Subsequent difference Fourier treatments [15] result in 53 additional atomic positions including eight for P, nine for Mg, six for Na and 30 for O. Among them, P(7), P(8), O(72), O(73), O(74), O(82), O(83), O(84) and Na(6) occupy general positions slightly displaced from the (0,y,z) mirror. Each of these atoms is denoted by its atomic name followed by the letter x, such as P(7)x. The refinement revealed that these atoms exhibit abnormally large thermal displacements. When their occupancy factors were allowed to refine, they all converged at approximately 0.5. Each of them was then modulated by two positions (left and right), symmetric by the (0,y,z) mirror. These positions cannot be filled simultaneously due to their too close location. A last cycle of refinement including all atomic coordinates and anisotropic thermal parameters converged at $R_1 = 0.025$ and w$R_2 = 0.059$ for the observed reflections $[F_o^2 > 4\sigma(F_o^2)]$.

Atomic coordinates and equivalent isotropic temperature factors $U_{eq.}$ for $Na_7Mg_{13}Eu(PO_4)_{12}$ are reported in Table 3. The structure exhibits a new three-dimensional framework that has never been observed up to now. It consists of an assemblage of EuO_8, MO_6 ($M = 0.5Mg + 0.5Na$) and MgO_x ($x = 5$, 6) polyhedra linked either directly through common corners, edges or faces or

by means of the phosphate tetrahedra, the Na^+ cations being located in large interstitial cavities (Fig. 2). The framework is well described when projected along the c-axis (Fig. 3). From this projection, one can formally isolate two main building blocks: $[Mg_4MP_4O_{22}]_\infty$ layers stacked along a and $[Mg_4EuP_4O_{36}]_\infty$ undulating chains spreading along b. Successive $[Mg_4MP_4O_{22}]_\infty$ layers are equivalent by the $(0, y, z)$ mirror being interconnected via common edges of $Mg(7)O_5$ polyhedra (Fig. 3). One layer is depicted separately in Fig. 4. It is an alternate assemblage of $[Mg_2P_2O_{12}]_\infty$ chains and $[Mg_2MP_2O_{14}]_\infty$ ribbons which are both running along b. The $[Mg_2P_2O_{12}]_\infty$ chains are formed by Mg_2O_9 units of edge-sharing $Mg(5)O_6$ and $Mg(8)O_5$ polyhedra, linked by the $P(1)O_4$ and $P(2)O_4$ tetrahedra. Each tetrahedron connects two neighboring units either by sharing one apex with each unit $(P(1)O_4)$ or by sharing one edge with one unit and one apex with the other $(P(2)O_4)$ (Fig. 4b).

The $[Mg_2MP_2O_{14}]_\infty$ ribbons are consisted by MMg_2O_{13} trinuclear cyclic units in which one $Mg(7)O_5$ polyhedron is corner-linked to one MO_6 and one $Mg(6)O_5$ polyhedra. The latter two polyhedra are also corner-connected. Two successive units are linked in the b direction by the $P(3)O_4$ and $P(4)O_4$ tetrahedra. $P(3)O_4$ shares one apex with one unit and one edge with the other while $P(4)O_4$ is edge-linked to each unit (Fig. 4c).

The second building block of the framework, i.e., the $[Mg_4EuP_4O_{36}]_\infty$ undulating chain is consisted of EuO_8, $Mg(1)O_5$ and $Mg(4)O_6$ isolated polyhedra and Mg_2O_9 bioctahedral units arising from a face-sharing between $Mg(2)O_6$ and $Mg(3)O_6$ octahedra. The connexion of these structural units being ensured by the $P(5)O_4$, $P(6)O_4$, $P(7)xO_4$ and $P(8)xO_4$ tetrahedra (Fig. 5).

The three-dimensional architecture built up by the connection between the layers and the undulating chains forms six symmetry distinct cavities occupied by the Na^+ cations.

Main interatomic distances are given in Table 4.

Table 3
Atomic coordinates and equivalent isotropic thermal parameters U_{eq}.

| Atom	Wyckoff	Occupancy	$x(\sigma)$	$y(\sigma)$	$z(\sigma)$	U_{eq}
Eu	4a	1	0	0.4552(1)	0.9995(1)	0.0076(1)
Mg(1)	4a	1	0	0.5975(2)	0.7202(2)	0.0091(5)
Mg(2)	4a	1	0.5	0.5615(2)	0.8697(2)	0.0066(5)
Mg(3)	4a	1	0	0.1475(2)	0.9836(2)	0.0073(5)
Mg(4)	4a	1	0	0.2168(2)	0.6052(2)	0.0123(5)
Mg(5)	8b	1	0.2385(2)	0.7015(2)	0.8249(1)	0.0087(3)
Mg(6)	8b	1	0.7686(3)	0.3596(2)	0.5694(1)	0.0311(7)
Mg(7)	8b	1	0.6542(2)	0.3909(2)	0.7129(1)	0.0178(4)
Mg(8)	8b	1	0.7554(2)	0.3824(2)	0.8819(1)	0.0151(4)
(Mg, Na)	8b	0.5(1),0.5(2)	0.7554(3)	0.4308(2)	0.1241(1)	0.0287(6)
Na(1)	4a	1	0	0.9065(3)	0.2195(2)	0.0188(7)
Na(2)	4a	1	0	0.7347(3)	0.5982(2)	0.0214(8)
Na(3)	4a	1	0	0.5469(3)	0.8558(2)	0.0213(9)
Na(4)	4a	1	0.5	0.5682(2)	0.4780(2)	0.0226(8)
Na(5)	4a	1	0.5	0.2242(3)	0.9457(2)	0.033(1)
Na(6)x	8b	0.500	0.0319(7)	0.3510(5)	0.7630(3)	0.048(3)
P(1)	8b	1	0.7814(2)	0.5677(1)	0.9412(1)	0.0048(2)
O(11)	8b	1	0.8184(4)	0.6415(2)	0.9010(2)	0.0117(7)
O(12)	8b	1	0.6342(4)	0.5531(2)	0.9445(2)	0.0110(7)
O(13)	8b	1	0.8452(3)	0.5803(2)	0.0002(2)	0.0116(6)
O(14)	8b	1	0.8482(4)	0.4828(2)	0.9203(2)	0.0103(7)
P(2)	8b	1	0.2529(2)	0.5355(1)	0.7785(1)	0.0090(2)
O(21)	8b	1	0.2268(5)	0.4489(3)	0.8060(2)	0.024(2)
O(22)	8b	1	0.2895(4)	0.5178(3)	0.7161(2)	0.0188(9)
O(23)	8b	1	0.1339(4)	0.5955(2)	0.7829(2)	0.0102(7)
O(24)	8b	1	0.3610(4)	0.5890(3)	0.8086(2)	0.0119(8)
P(3)	8b	1	0.7548(2)	0.2985(1)	0.0138(1)	0.0081(3)
O(31)	8b	1	0.7004(4)	0.3300(3)	0.9573(2)	0.0160(8)
O(32)	8b	1	0.6405(4)	0.2627(3)	0.0488(2)	0.0163(8)
O(33)	8b	1	0.8485(4)	0.2210(2)	0.0123(2)	0.0158(8)
O(34)	8b	1	0.8253(4)	0.3731(2)	0.0454(2)	0.0160(8)
P(4)	8b	1	0.7611(2)	0.2733(1)	0.1809(1)	0.0113(3)
O(41)	8b	1	0.6370(5)	0.3172(4)	0.1613(3)	0.037(2)
O(42)	8b	1	0.7525(6)	0.2395(3)	0.2422(2)	0.027(2)
O(43)	8b	1	0.8685(4)	0.3408(3)	0.1714(2)	0.0148(8)
O(44)	8b	1	0.7972(5)	0.1929(3)	0.1450(2)	0.021(1)
P(5)	4a	1	0	0.2766(2)	0.8852(1)	0.0054(3)
O(51)	4a	1	0	0.3372(3)	0.9360(3)	0.012(2)
O(52)	4a	1	0	0.1819(3)	0.9023(2)	0.009(1)
O(53)	8b	1	0.8787(4)	0.2932(2)	0.8482(2)	0.0117(7)
P(6)	4a	1	0.5	0.3517(2)	0.8300(1)	0.0062(3)
O(61)	4a	1	0.5	0.3766(4)	0.7673(3)	0.016(2)
O(62)	8b	1	0.3799(4)	0.2994(3)	0.8455(2)	0.0187(9)
O(63)	4a	1	0.5	0.4316(4)	0.8684(3)	0.031(2)
P(7)x	8b	0.500	0.9735(2)	0.4425(2)	0.6359(2)	0.0061(7)
O(71)	4a	1	0	0.4685(4)	0.6981(2)	0.013(2)
O(72)x	8b	0.500	0.0248(11)	0.3526(5)	0.6228(4)	0.023(3)
O(73)x	8b	0.500	0.9427(8)	0.5055(6)	0.5992(4)	0.017(2)
O(74)x	8b	0.500	0.8304(7)	0.4526(6)	0.6177(4)	0.017(2)
P(8)x	8b	0.500	0.4825(8)	0.4699(2)	0.6004(2)	0.011(2)
O(81)	4a	1	0.5	0.4374(6)	0.6613(3)	0.027(2)
O(82)x	8b	0.500	0.5516(7)	0.4080(5)	0.5590(3)	0.011(2)
O(83)x	8b	0.500	0.6667(8)	0.4692(5)	0.5901(4)	0.012(2)
O(84)x	8b	0.500	0.4644(10)	0.5607(6)	0.5919(5)	0.043(4)
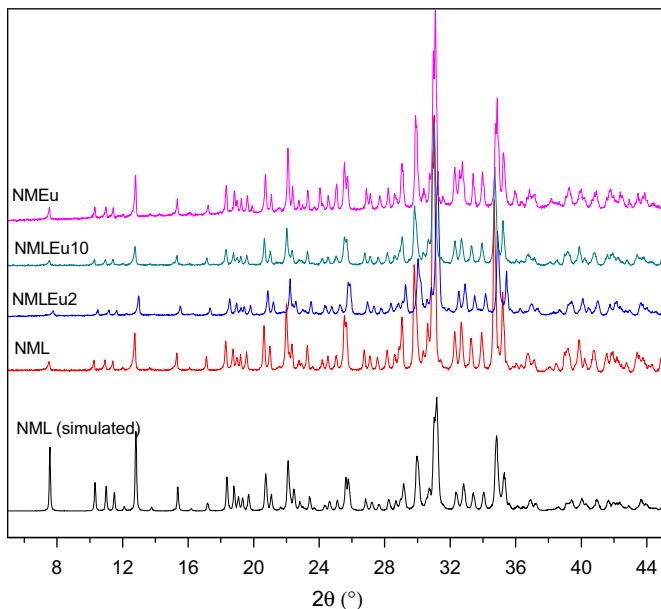
Fig. 1. The observed X-ray patterns for the NML, NMLEu2, NMLEu10, NMEu samples together with the simulated one for NML.

Table 2
Cell parameters and volume of $Na_7Mg_{13}La_{1-x}Eu_x(PO_4)_{12}$ determinated from powder diffraction.

Parameters	$Na_7Mg_{13}La(PO_4)_{12}$	$Na_7Mg_{13}La0.98Eu0.02(PO_4)_{12}$	$Na_7Mg_{13}La0.9Eu0.1(PO_4)_{12}$	$Na_7Mg_{13}Eu(PO_4)_{12}$
a (Å)	10.327(1)	10.331(1)	10.320(1)	10.270(1)
b (Å)	15.458(1)	15.458(1)	15.462(1)	15.455(1)
c (Å)	23.390(1)	23.381(1)	23.395(1)	23.416(1)
V (Å^3)	3733.96(16)	3734.08(3)	3733.18(3)	3716.76(3)
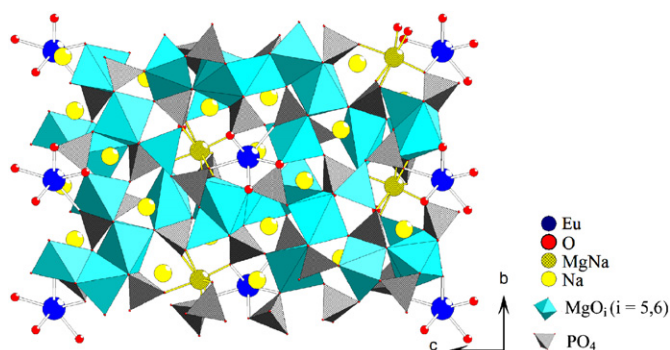
Fig. 2. A projection of the $Na_7Mg_{13}Nd(PO_4)_{12}$ structure along the a-axis.
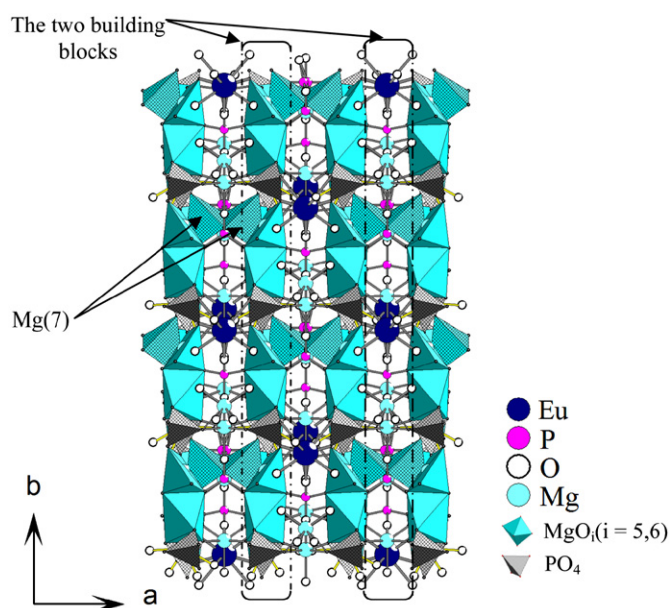
Fig. 3. A projection of the $Na_7Mg_{13}Eu(PO_4)_{12}$ along the c-axis.

Fig. 4. (a) The $[Mg_4MP_4O_{22}]_\infty$ layer, (b) the $[Mg_2P_2O_{12}]_\infty$ chain and (c) the $[Mg_2MP_2O_{14}]_\infty$ ribbon.

Fig. 5. $[Mg_4EuP_4O_{36}]_\infty$ undulating chain.

3.1.1. Europium environment

The only distinct Eu atom is coordinated by eight O atoms with Eu–O distances in the range 2.353(5)–2.503(3) Å (Fig. 6a). The mean distance of 2.456 Å is in accordance with that 2.415 Å observed for the eight coordinated Eu^{3+} in EuP_5O_{14} [16].

3.1.2. Magnesium/sodium environment

The M (M=0.5Mg+0.5Na) site is the only disordered one in the structure. Its environment is apparently consisted by eight O atoms. However, the central atom is connected only to one of O(73)x and O(74)x atoms whether the P(7)x orientation is left (O(73)x) or right (O(74)x) and similar observation can be done for the O(83)x and O(84)x atoms (Fig. 6b). Thus, the environment is effectively constituted by six O atoms with an average M–O distance of 2.20(2) Å, close to 2.230 Å reported for the disordered M (M=0.5Mg+0.5Na) site in the molybdate $Na_2Mg_5(MoO_4)_6$ [17].

Among the eight distinct Mg atoms contained in this structure, Mg(2) to Mg(5) are six coordinated with Mg–O distances varying from 1.934(8) to 2.459(10) Å with an overall distance of 2.098 Å, somewhat less than 2.14 Å, observed for octahedral Mg^{2+} ions in $Mg_3(PO_4)_2$ [18]. It can be noticed that the $Mg(4)O_6$ octahedron exhibits one extremely long distance [(Mg(4)–O(84)x=2.459(10) Å)] compared to the others (from 1.980(4) to 2.154(8) Å). Thus, this environment can be considered as [5 +1]. Similar environment has already been observed in $Mg_3(PO_4)_2$ [18].
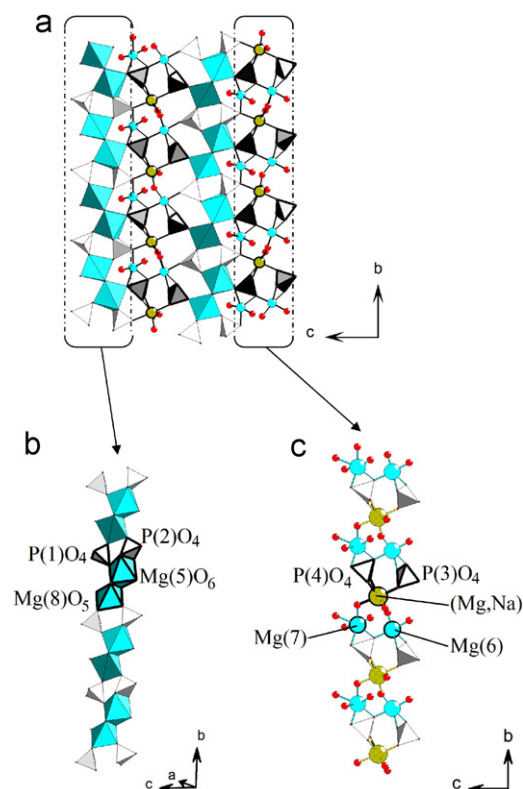
The environment of the Mg(6) atom also apparently consists of six oxygen atoms. However, its connectivity to each of the O(74)x and O(83)x atoms occurs with a probability of 1/2 (Fig. 6c). Consequently Mg(6) is effectively coordinated by only five O atoms having an average Mg(6)–O distance of 2.085 Å. Mg(1), Mg(7) and Mg(8) are five-coordinated with Mg–O distances in the range 2.008(4)–2.335(6) Å leading to an overall value of 2.087(6) Å, close to that 2.08 Å reported for the five-coordinated Mg^{2+} ion in $NaMg_4(PO_4)_3$ [19]. The occurrence of one large Mg(7)–O distance (2.335(6) Å) when compared to the four others shows the Mg(7) environment to be of [4 +1] type.

The environments of the Na^+ cations were determined assuming a maximum cation–oxygen distance L_{max}=3.13 Å, according to Donnay and Allmann [20]. Accordingly, their coordination numbers vary from 5 to 10 with Na–O distances scattering from 2.316(5) to 3.016(6) Å.

Table 4
Selected interatomic distances for $Na_7Mg_{13}Eu(PO_4)_{12}$.

Eu–O(51) 2.353(5)	Mg(8)–O(31) 2.020(4)	P(1)–O(11) 1.525(4)
Eu–O(34) 2.446(4)x2	Mg(8)–O(14) 2.030(4)	P(1)–O(12) 1.532(4)
Eu–O(14) 2.459(4)x2	Mg(8)–O(53) 2.030(4)	P(1)–O(13) 1.538(5)
Eu–O(73)x 2.479(8)	Mg(8)–O(21) 2.059(5)	P(1)–O(14) 1.559(4)
Eu–O(13) 2.503(3)x2	Mg(8)–O(62) 2.075(5)	< P(1)–O > **1.538**
< Eu–O > **2.456**	< Mg(8)–O > **2.043**	
		P(2)–O(21) 1.508(4)
Mg(1)–O(43) 2.008(4)x2	(Mg,Na)–O(83)x 1.961(8)x0.5	P(2)–O(22) 1.532(4)
Mg(1)–O(23) 2.011(5)x2	(Mg,Na)–O(74)x 1.962(9)x0.5	P(2)–O(23) 1.538(4)
Mg(1)–O(71) 2.059(6)	(Mg,Na)–O(43) 2.124(5)	P(2)–O(24) 1.552(4)
< Mg(1)–O > **2.019**	(Mg,Na)–O(34) 2.167(5)	< P(2)–O > **1.532**
	(Mg,Na)–O(73)x 2.238(9)x0.5	
Mg(2)–O(63) 2.007(6)	(Mg,Na)–O(41) 2.307(7)	P(3)–O(31) 1.516(4)
Mg(2)–O(52) 2.009(5)	(Mg,Na)–O(22) 2.339(5)	P(3)–O(32) 1.534(4)
Mg(2)–O(24) 2.065(4)x2	(Mg,Na)–O(84)x 2.385(12)x0.5	P(3)–O(33) 1.536(4)
Mg(2)–O(12) 2.230(4)x2	< (Mg,Na)–O > **2.185**	P(3)–O(34) 1.548(4)
< Mg(2)–O > **2.101**		< P(3)–O > **1.533**
	Na(1)–O(41) 2.395(6)x2	
Mg(3)–O(52) 1.975(6)	Na(1)–O(22) 2.459(5)x2	P(4)–O(41) 1.516(5)
Mg(3)–O(82)x 2.030(7)	Na(1)–O(24) 2.528(5)x2	P(4)–O(42) 1.530(5)
Mg(3)–O(33) 2.040(4)x2	Na(1)–O(81) 2.767(9)	P(4)–O(43) 1.533(4)
Mg(3)–O(12) 2.206(4) x2		P(4)–O(44) 1.544(4)
< Mg(3)–O > **2.083**	Na(2)–O(43) 2.474(5) x2	< P(4)–O > **1.531**
	Na(2)–O(44) 2.606(6) x2	
Mg(4)–O(32) 1.980(4) x2	Na(2)–O(33) 2.631(5) x2	P(5)–O(51) 1.511(6)
Mg(4)–O(41) 1.994(5) x2	Na(2)–O(34) 2.742(6) x2	P(5)–O(52) 1.517(5)
Mg(4)–O(72)x 2.154(8)	Na(2)–O(82)x 2.880(9) x2	P(5)–O(53) 1.539(4) x2
Mg(4)–O(84)x 2.459(10)		< P(5)–O > **1.526**
< Mg(4)–O > **2.093**	Na(3)–O(23) 2.316(5) x2	
	Na(3)–O(14) 2.385(5) x2	P(6)–O(61) 1.516(6)
Mg(5)–O(62) 1.999(5)	Na(3)–O(11) 2.595(5) x2	P(6)–O(62) 1.519(4) x2
Mg(5)–O(11) 2.090(4)	Na(3)–O(21) 3.014(6) x2	P(6)–O(63) 1.525(6)
Mg(5)–O(53) 2.092(4)		< P(6)–O > **1.519**
Mg(5)–O(42) 2.140(5)	Na(4)–O(12) 2.454(5) x2	
Mg(5)–O(24) 2.179(4)	Na(4)–O(63) 2.563(8)	P(7)x–O(72)x 1.516(8)
Mg(5)–O(23) 2.192(4)	Na(4)–O(31) 2.634(5) x2	P(7)x–O(71) 1.532(6)
< Mg(5)–O > **2.115**	Na(4)–O(84)x 2.690(13) x2	P(7)x–O(74)x 1.539(8)
		P(7)x–O(73)x 1.557(9)
Mg(6)–O(74)x 1.934(8)x0.5	Na(5)–O(11) 2.490(5) x2	< P(7)x–O > **1.536**
Mg(6)–O(13) 2.026(5)	Na(5)–O(31) 2.643(5) x2	
Mg(6)–O(83)x 2.047(8)x0.5	Na(5)–O(32) 2.874(6) x2	P(8)x–O(84)x 1.517(9)
Mg(6)–O(44) 2.059(5)	Na(5)–O(62) 2.890(7) x2	P(8)x–O(81) 1.521(8)
Mg(6)–O(32) 2.163(4)	Na(5)–O(13) 3.016(6) x2	P(8)x–O(82)x 1.535(8)
Mg(6)–O(33) 2.188(5)		P(8)x–O(83)x 1.552(11)
< Mg(6)–O > **2.069**	Na(6)x–O(53) 2.369(7)	< P(8)x–O > **1.531**
	Na(6)x–O(71) 2.389(8)	
Mg(7)–O(22) 2.044(5)	Na(6)x–O(53) 2.692(8)	
Mg(7)–O(61) 2.045(5)	Na(6)x–O(21) 2.704(9)	
Mg(7)–O(44) 2.109(5)	Na(6)x–O(42) 2.707(9)	
Mg(7)–O(81) 2.117(6)		
Mg(7)–O(42) 2.335(6)		
< Mg(7)–O > **2.130**		

3.1.3. Phosphor environment

The P–O distances and the O–P–O intra-tetrahedral angles within the eight distinct PO_4 tetrahedra are in the ranges 1.508(4)–1.559(4) Å and 109.36(2)–109.59(4)° with overall values of 1.531 Å and 109.45°, respectively. Such values are reported in anhydrous monophosphates [21]. As indicated in the structural determination section, both the P(7)x and P(8)x phosphorus are slightly removed from the (0,y,z) mirror, being statistically occupying two symmetric positions: left and right (Fig. 6a). The removing of these atoms from the mirror probably occurs as a result of the need to accommodate the environments of neighboring Eu and M sites. In fact, the constraint of the P(7)x atom to occupy the mirror results in an abnormally short Eu–P distance (dEu–P(7)x = 3.57 Å).

3.2. Optical study

In this study, the four samples synthesized as powders, namely (NML), (NMLEu2), (NMLEu10) and (NMEu) were analyzed. The

four samples were, first of all, analyzed by diffused reflectance in the same condition. Results are shown in Fig. 7.

3.2.1. Diffuse reflectance

The diffuse reflectance spectrum of the un-doped sample NML reveals a large absorption band up to 370 nm. Knowing that the usual host band (corresponding to the transition between the valence band and the conduction band) of phosphates occurs at higher energies (wavelength below 250 nm) [12], this band cannot be attributed only to the host only. So this phenomenon can be explained by the absorption of the incident light by various defaults $\Phi 1$ (electron–hole trap, colored center, structural default, etc.) or by other charge transfer bands (CTB) (La–O, etc.).

Replacing progressively lanthanum by europium modifies drastically the diffuse reflectance characteristics. First of all, there is a global increase of the overall reflection above 380 nm with a maximum reaching almost 100% for the three europium content compounds. This increase, compared to the un-doped sample, is
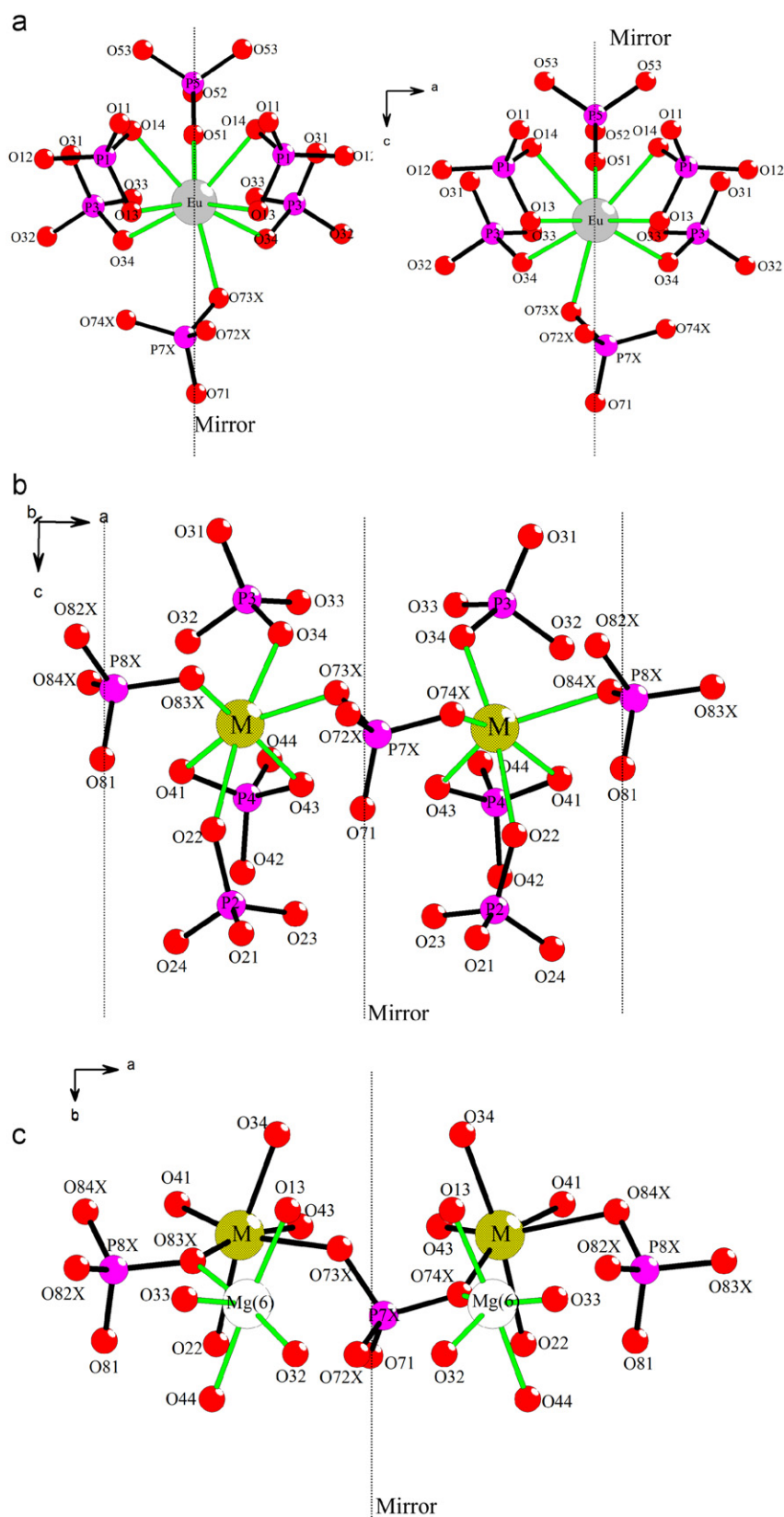
Fig. 6. (a) The left and right orientations of the P(7)xO$_4$ tetrahedron around the Eu site. (b) The left and right orientations of P(7)x and P(8)x around M site; (c) The tow environments of Mg(6) site.

more effective over the full wavelength range especially as the La/Eu substitution is complete. It could be explained by the annihilation of a structural default as a result of a structural rearrangement induced by the replacement of La^{3+} (r_i=1.09 Å) by

Eu^{3+} (r_i=0.95 Å). As noted in the previous crystallographic study, the *Ln* site is strained causing a displacement of the P(7)x atom from the (0,y,z) mirror. This strain seems to be decreased when the La^{3+} cation is replaced by the smaller Eu^{3+} cation.
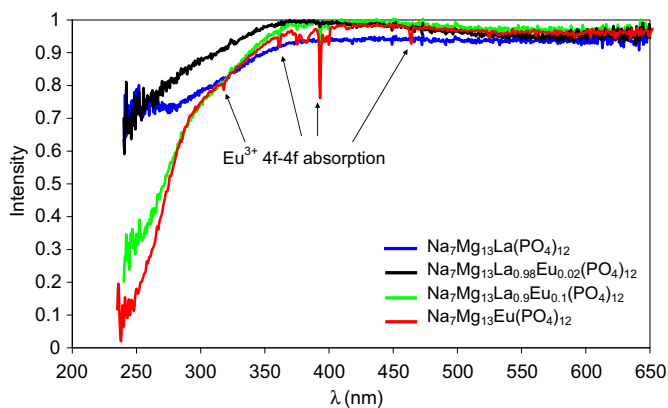
Fig. 7. Diffuse reflectance spectra of samples NML, NMLEu2, NMLEu10, NMEu.

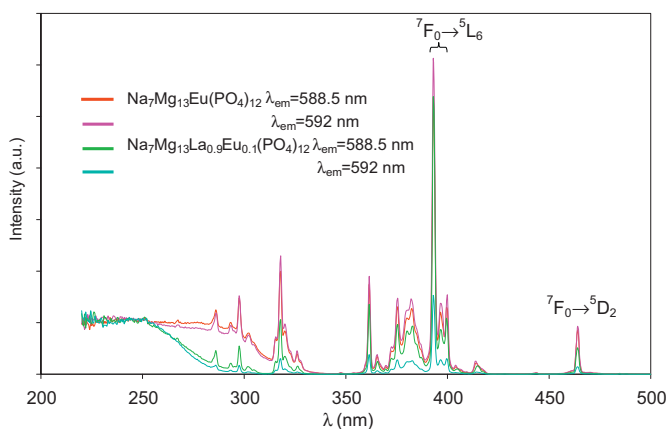**Fig. 8.** Normalized (at 240 nm) excitation spectra of NMEu sample and NMEu10 compounds for $\lambda_{em}=588.5$ and 592 nm.

Then the substitution La→Eu modifies the absorption band below 380 nm. The absorption band previously described and attributed to Φ_1 defects decreases with the increase of the europium concentration. Simultaneously, Eu–O charge transfer bands (CTB) clearly appear below 300 nm [22]. On the spectra, two main bands can be identified at around 250 and 280 nm. Their contribution to the global absorption increases by modifying the La→Eu substitution rate. Finally, the 4f–4f absorption lines of trivalent europium are visible at 362, 375, 393 and 464 nm. Their intensity varies with the europium concentration.

3.3. Photoluminescence

Figs. 8 and 9 represent the excitation and emission spectra of the NMEu (crushed crystal) and NMLEu10 materials. For the NMEu europium phosphate, excitation spectra reveal the existence of two large bands whatever the selected emission wavelength. Regarding the contribution of these bands to the radiative emission, one can note that their intensities are surprisingly low compared to the contribution of the forbidden 4f–4f absorption lines. This might be due to a configurational quenching: a large part of the excitation energy relaxes non-radiatively from the charge transfer state (CTS) to the fundamental multiplet ^7F_J. This has already been observed in phosphate and oxyphosphates, which present CTB at low energy [23]. A small difference can be noticed in the relative intensity of the CTB for the selected emission wavelength.

For the 10% europium content, strong modifications can be noticed. The low energy CTB is not detected anymore (it is very weak) on the excitation spectra for both emission values. This can be due to re-absorption phenomena by the Φ_1 band and/or less amount of europium in site corresponding to Eu–O bonds of low energy CTB. This is in a good agreement with the relative intensities of the CTB detected on the diffuse reflectance spectra.

The excitation spectra were normalized on the maximum of the CTB. The relative intensity between the CTB and the 4f lines traduces the contribution of the band to the radiative emission. Considering the first tests, two emission wavelengths have been selected. For the NMEu compound, no significant modification of the excitation spectra can be noticed. For the NMLEu10 compound, strong modifications are observed. For $\lambda_{em}=592$ nm, the intensity of the CTB located at 250 nm is in the same order of magnitude than the intensity of the 4f lines at around 394 nm. For $\lambda_{em}=588.5$ nm, the contribution of the 4f line is much higher than that of the CTB indicating that these two emission lines do not result from de-excitation processes via the same CTS. For this second emission wavelength, a higher configurational quenching of the CTB occurs. By consequence, this selected emission wavelength results from de-excitation processes implying the lowest energy CTS. Same results have been obtained for the 2% europium content.

Emission spectra were collected for excitation in the different CTB and the 4f absorption lines. For the europium phosphate compound NMEu, no modification of the spectral distribution is
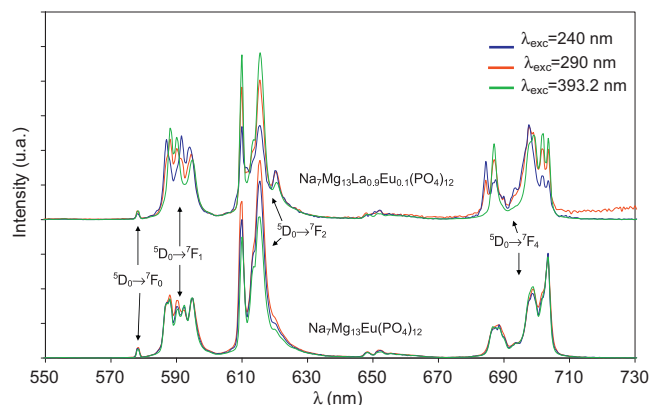

Fig. 9. Normalized (at 595 nm) emission spectra of NMEu sample and NMEu10 compounds for $\lambda_{exc}=240$, 290 and 393.2 nm.
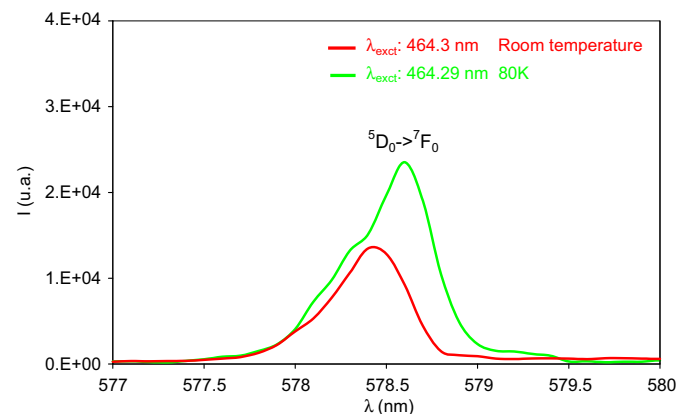

Fig. 10. $^5D_0 \rightarrow {^7F_0}$ Low temperature photoluminescent emission spectra of sample NMEu:Na$_7$Mg$_{13}$Eu(PO$_4$)$_{12}$.

observed for excitation in the CTB or in the 4f lines. The main part of emission is due to the $^5D_0 \rightarrow {}^7F_2$ electric dipole transition, located in the red part of the electromagnetic range. These transitions also named hypersensitive transitions, revealed the location of europium in an environment without inversion center. The ratio $I_{^5D_0-^7F_2}/I_{^5D_0-^7F_1}$ is generally used to characterize this phenomenon [2]. On the spectra (Fig. 9) at least 5 lines attributed to the $^5D_0 \rightarrow {}^7F_1$ magnetic dipole transition can be observed. This reflects the location of the europium ions in at least two coordination polyhedra, which is coherent with the existence of the two CTB previously described. The lack of spectral modification for excitation at 240, 290 or 393 nm indicates that the collected emission is mainly due to the lowest energy site due to energy transfer between these two sites. In this case, the distortion of the lowest energy site favours a configurational mixing giving rise to an increase of the electric dipole transition probability. Moreover two factors have to be considered: first, at room temperature a thermal equilibrium may exist between both sites (emitting level at very close energy). Secondly, the quantity of europium ions located in the site associated to the highest energy CTB is bigger. These two arguments make possible the observation of the two types of luminescence. To confirm the fact the europium ions occupied two types of coordination polyhedra, liquid nitrogen temperature measurements were performed. Fig. 10 clearly shows the presence of two $^5D_0$-$^7F_0$ singlet–singlet transition. This cannot be due to the presence of any impurity since the measurements were done on crushed crystals.

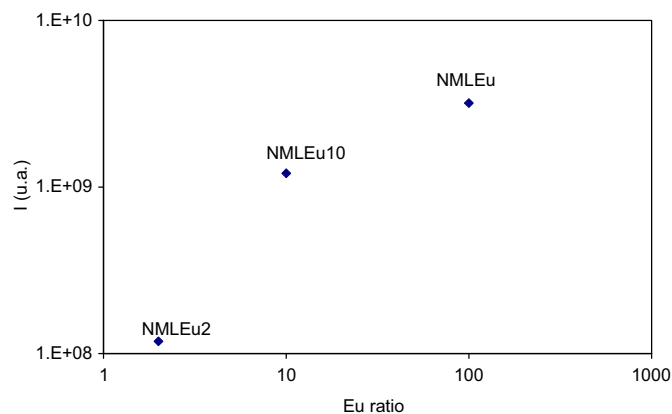**Fig. 11.** Relative intensity of the integrated emission spectrum (λ_{exc}=393 nm) of NMLEu2, NMLEu10 and NMEU samples.
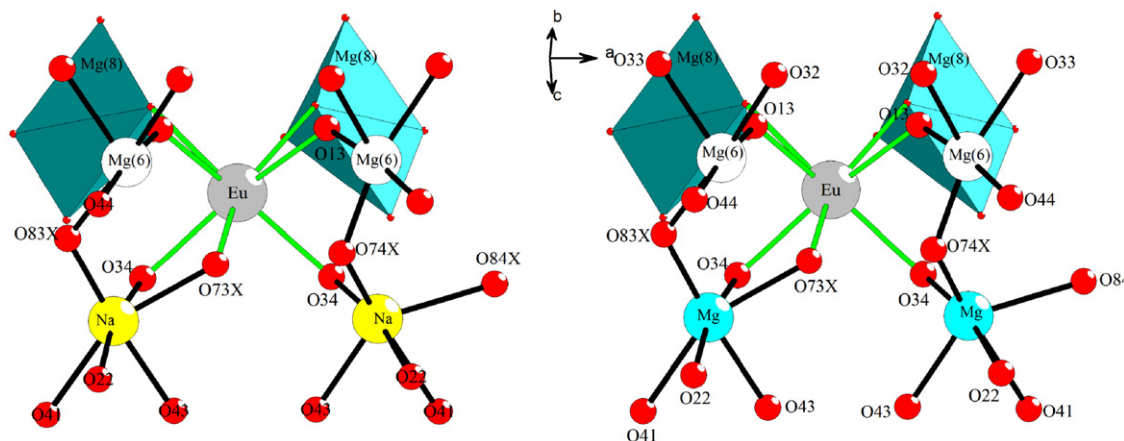
The situation is slightly different for the 10% europium content. At room temperature, quite selective excitations have been performed on this compound leading to the observation of two distinct emission spectra. An excitation at 240 nm in the high energy CTB gives rise to an orange emission (top of Fig. 9). The relative intensity between the magnetic and electric dipole transition is quite the same. The red emission already described for the NMEu europium phosphate is obtained for an excitation in the 4f lines. In this case, the corresponding CTB is not so efficient because of the re-absorption due to the $\Phi 1$ band, the configurational quenching through the CTB down to the fundamental multiplet and the probably minor quantity of europium location in these sites. Same observations have been made for the 2% europium content compound.

Finally, the integrated emission for an excitation at 393 nm is represented in Fig. 11. It reveals that the concentration quenching of the europium in this materials is quite low. In fact, considering the structural description, a100% europium content corresponds to about 10^{20} ions/cm³. This will limit the energy transfer from the excited europium ions to killer centers.

3.3.1. Discussion

Luminescence spectra recorded on all the samples clearly revealed the location of the europium in two environments. Considering the crystallographic data, a unique position is expected for the europium ions, with two surrounding environments in the second coordination sphere. The substitution of Mg by Na (Fig. 12) in the second coordination sphere of the rare earth element is enough to introduce a small disorder around the rare earth element but it cannot explain the strong modification observed on the emission spectra of the La/Eu compounds.

Several hypotheses can be formulated. First, a structural rearrangement may result from the constraint related to the cationic radii difference between La^{3+} and Eu^{3+} ions. Secondly, the europium element may occupy sodium-ion sites. A quantity of the rare earth element in this unexpected site is too small to be detected by the X-ray diffraction. Moreover a strong change in the local symmetry could explain the difference in the Stark component splitting of the europium ions. The crystallographic data indicate that the natural europium ion location is associated with eightfold coordination polyhedra. Considering the relative intensity of the CTB on the diffuse reflectance spectra and the emission and excitation spectra, one can suppose that the natural europium luminescence is associated with the orange spectral distribution (maximum of the CTB at about 240 nm). The red luminescence is then favoured by a strong mixing of the orbital due to local distortion in the rare earth environment (CTB at

Fig. 12. The two local Eu environments whether the M site is occupied by Na or Mg.

280 nm). This could result from the location of the europium in a sodium site. Even if the sodium and europium are different in size and in charge, their substitution was already observed in borate, phosphate and bromide compounds with large polyhedra [24–28]. Creation of local disorder between the Eu–Na distributions in the array could make possible the observation of the secondary emission. One can also imagine local charge compensation with creation of cationic vacancy to compensate the excess of positive charge in a sodium position.

The last observation concerns the relative intensity of the CTB/4f lines. The low intensity of the CTB (in Fig. 8) means that the light absorbed by the CTS (seen in Fig. 7) is not totally transformed in radiative emission. An important part of excited energy does not transfer to emitting 4f level and then does not imply a photoluminescent phenomenon. This is a direct consequence of the low energy position of CTS which allows a direct nonradiative deexcitation to the fundamental multiple [29]. This observation does not suppose a favorable opportunity for a potential application of these phosphates for LEDS, even if the diode-chips are providing an incoming light below 300 nm. But for diode emitting at the specific wavelength of the europium f–f transitions (362, 375, 393, 464 nm.), these materials could be promising for such purpose.

4. Conclusion

Two new rare earth phosphates $Na_7Mg_{13}Ln(PO_4)_{12}$ (Ln = La, Eu) have been synthesized and shown to exhibit an original structure built from LnO_8 (Ln = La, Eu), MO_6 (M = Mg, Na) and MgO_x (x = 5, 6) polyhedra and PO_4 tetrahedra linked by corner-, edge- and face-sharing. The 3D covalent framework is basically consisted of $[Mg_4MP_4O_{22}]_\infty$ layers stacked along the a direction. These layers are interconnected in the b direction by $[Mg_4LnP_4O_{32}]_\infty$ undulating chains, in such a way that the resulting skeleton forms six distinct cavities, occupied by the Na^+ cations.

The optical results obtained on $Na_7Mg_{13}La_{1-x}Eu_x(PO_4)_{12}$ ($0 \le x \le 1$) revealed the location of the europium in at least two different sites. In NMLEu10, two emission spectral distributions have been observed. The orange emission can be obtained for excitation in the CTB at 240 nm. An attribution of the orange emission to the natural europium site seems to be coherent with the spectroscopic data but further experimentations with more specific laser excitation at low temperature would be necessary to identify the local symmetry around the rare earth element. For the NMEu europium phosphate energy transfer occurs between both sites leading to a global red emission.

Appendix A. Supplementary material

References

[1] T. Kanazawa, Inorganic Phosphate Materials, Kodansha, Tokyo, Japan, 1989.
[2] G. Blasse, B.C. Grabmaier, Luminescent Materials, Springer, New York, 1994.
[3] M.I. Baraton, Int. J. Nanotech. 6 (9) (2009) 776.
[4] S.F. Wang, R.K. Koteswara, Y.C. Wu, Y.R. Wang, Y.F. Hsu, C.Y. Huang, Int. J. Appl. Ceram. Technol. 6 (2008) 470.
[5] E. Mihokova, M. Nikl, J.A. Mares, A. Beitlerova, A. Vedda, K. Nejezchleb K. Blazek, C. D'Ambrosio, J. Lumin. 126 (2007) 77.
[6] S.K. Singh, A.K. Singh, D. Kumar, O. Prakash, S.B. Rai, Appl. Phys B Las. Opt. 98 (2010) 173.
[7] P.C. De Sousa, O.A. Serra, J. Lumin. 129 (2009) 1664.
[8] C.C. Lin, Y.S. Tang, S.F. Hu, R.S. Liu, J. Lumin. 129 (2009) 1682.
[9] P. Thiyagarajan, M. Kottaisamy, K. Sethupathi, M.S.R. Rao, Displays 30 (2009) 202.
[10] Y.L. Huang, C.F. Jiang, Y.G. Cao, L. Shi, H.J. Seo, Mater. Res. Bull. 44 (2009) 793.
[11] R.A. Benhamou, A. Bessiere, G. Wallez, B. Viana, M. Elaatmani, M. Daoud A. Zegzouti, J. Solid State Chem. 182 (2009) 2319.
[12] C.T. Dinh, P.V. Huong, R. Olazeuaga, C. Fouassier, J. Opt. Adv. Mater. 2 (2000) 159.
[13] M.P. Pechini, US Patent No. 3.33, 1967, p. 679.
[14] A. Altomare, G. Cascarano, C. Giacovazzo, A. Guagliardi, J. Appl. Crystallogr. 26 (1993) 343.
[15] G.M. Sheldrick, SHELXL97, A Program for the Solution of the Crystal Structures, University of Göttingen, 1997.
[16] J.M. Cole, M.R. Lees, J.A.K. Howard, R.J. Newport, G.A. Saunders, E. Schoenherr, J. Solid State Chem. 150 (2000) 377.
[17] R.F. Klevtsova, B.G. Kim, P.N. Klevtsov, Kristallografiya 25 (1980) 1148.
[18] S. Jaulmes, A. Elfkir, M. Quarton, F. Brunet, C. Chopin, J. Solid State Chem. 129 (1997) 341.
[19] M. Ben Amara, M. Vlasse, R. Olazcuaga, G. Le Flem, P. Hagenmuler, Acta Crystallogr. C 39 (1983) 936.
[20] G. Donnay, R. Allmann, Am. Mineral. 55 (1970) 1003.
[21] W.H. Baur, Acta Cryst. B 30 (1974) 1195.
[22] F. Khlissa, M. Ferid, M.C. Pujol, X. Mateos, J.J. Carvajal, F. Diaz, M. Aguilo, J. Cryst. Growth 311 (2009) 4360.
[23] D.C. Tuan, R. Olazcuaga, F. Guillen, A. Garcia, B. Moine, C. Fouassier, J. Phys. IV 123 (2005) 259.
[24] C. Cascales, R. Balda, V. Jubera, J.P. Chaminade, J. Fernández, Opt. Express 16 (2008) 2653.
[25] A.I. Orlova, D.B. Kitaev, D.V. Kemenov, M.P. Orlova, G.N. Kazantsev S.G. Samoilov, V.S. Kurazhkovskaya, Radiochemistry 45 (2003) 103.
[26] B.I. Lazoryak, T.V. Strunenkova, E.A. Vovk, V.V. Mikhailin, I.N. Shpinkov A.Y. Romanenko, V.N. Schekoldin, Mater. Res. Bull. 31 (1996) 665.
[27] F. Erragh, A. Boukhari, A. Sadel, E.M. Holt, Acta Crystallogr. Sec. C 54 (1998) 1373.
[28] W. Gong, M. Gaune-Escard, Thermochem. Acta 496 (2009) 173.
[29] V. Jubera, J.P. Chaminade, A. Garcia, F. Guillen, C. Fouassier, J. Lumin. 101 (2003) 1.